STUDIA UNIVERSITATIS BABEŞ-BOLYAI, CHEMIA, LII, 2, 2007

DIOXYGEN ACTIVATION BY RIESKE DIOXYGENASES – COMPUTATIONAL STUDIES. 1. POSSIBLE CATALYTIC INTERMEDIATES

RADU SILAGHI-DUMITRESCU*

ABSTRACT. Density functional and semiempirical calculations were performed on the non-heme mononuclear iron active site of Rieske dioxygenases (RDO), and on complexes of this site with oxygen and activated oxygen species that have been implicated in the RDO catalytic cycle. Dioxygen binding to the high-spin ferrous center in RDOs is predicted to result in an S=2 side-on ferric-superoxo moiety, with a long O-O bond (1.36 Å). One-electron reduction of this species is predicted to result in an S=5/2 or S=3/2 side-on ferric-peroxo species. Protonation of this peroxo intermediate is predicted to result in an S=5/2 ferric-hydroperoxo species, which is predicted to readily isomerize to a perferryl-oxo-hydroxo. These results are consistent with model compound studies as well as with the recent crystal structures of dioxygen- and substrate-bound naphthalene dioxygenase.

INTRODUCTION

Rieske dioxygenases (RDO) are non-heme iron enzymes catalyzing the *cis*-1,2 di-hydroxylation of aromatic substrates by molecular oxygen and a reductant (typically one of the reduced pyridine nucleotides (NAD(P)H), inserting the equivalent of hydrogen peroxide and resulting in a non-aromatic dihydrodiol. (see Scheme 1).

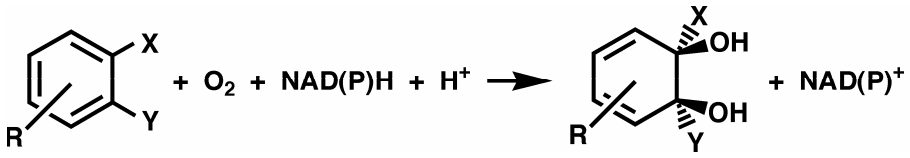

Scheme 1

* Department of Chemistry, "Babeş-Bolyai" University, Cluj-Napoca RO-400028, Romania

Mechanisms based on biochemical and model compound evidence proposed for the RDO-catalyzed reaction are shown in Figure 1.[1] In model compounds, ferric-hydroperoxo (Fe(III)-OOH) adducts are often found to undergo O-O bond cleavage forming higher-valent iron complexes (Fe(IV)=O, ferryl or Fe(V)=O, perferryl) with increased oxidative properties compared to the parent Fe(III)-OOH adducts.[1] While such chemistry is well-documented in heme enzymes, only one such high-valent intermediate has been identified in a non-heme iron oxygenase.[1] Of the ferrous-dioxygen, ferric-peroxo, ferric hydroperoxo and perferryl reaction intermediates proposed for RDOs, only the putative ferrous-dioxygen state of naphthalene dioxygenase (NDO) has been observed.[2]

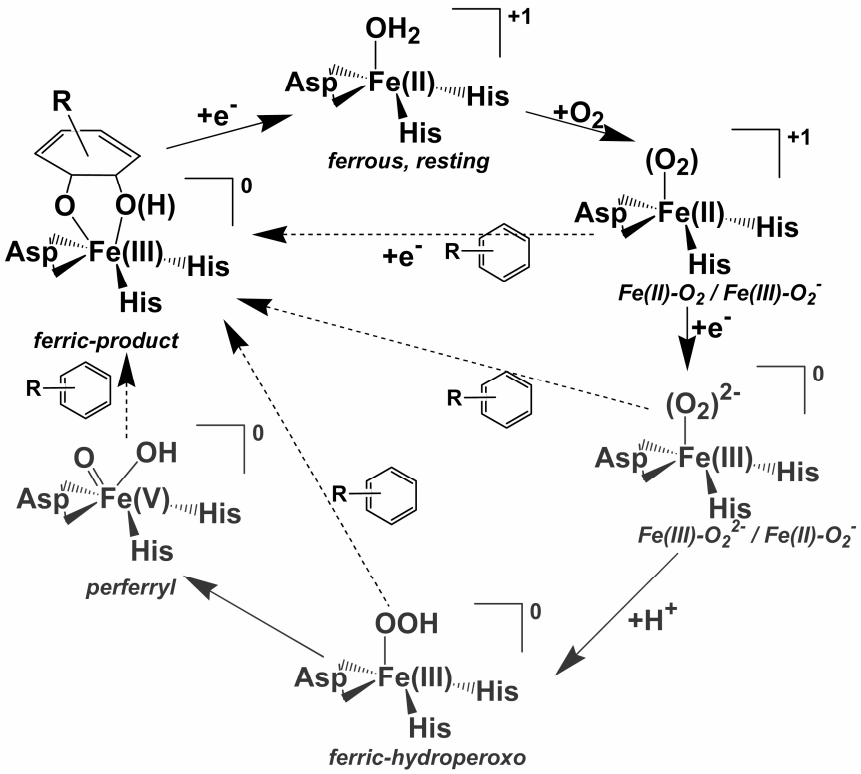

Figure 1. Proposed RDO catalytic mechanisms. Species shown in grey have never been observed in RDO. The identities of the protein-derived iron ligands are indicated. The aromatic substrate may be benzene (R = hydrogen), substituted benzenes, or other aromatics (including heterocyclic compounds).

In the present study DFT geometry optimizations were performed for models of RDO active site, as well as for various putative complexes of this active site with dioxygen and with activated dioxygen species, with the aim of predicting the most stable states – and thus the most important players in the still-elusive RDO catalytic cycle.

RESULTS AND DISCUSSION

The orientation of the protein-derived ligands changed dramatically upon unconstrained geometry optimization. These changes included reorientation of the carboxylate from semi-bidentate to clearly (symmetrically) bidentate, and rotations of the imidazole rings. Such changes are unlikely to be allowed at the active site, and attempts were made to avoid them. One option was to constrain Fe-ligand bond distances. However, this study attempts to examine and compare energies for various spin/oxidation states of putative reaction intermediates. Constraining Fe-ligand bond distances to the values seen in the crystal structure would artificially favor certain iron oxidation and/or spin states. Therefore, all protein-derived heavy atoms were kept frozen upon geometry optimization, in all models. The iron and the exogenous ligand (water, oxygen, peroxide, etc.), as well as all hydrogen atoms, were not frozen upon geometry optimization. This approach allowed the Fe-ligand distances to adjust in each model to a satisfactory degree, accommodating well any changes in spin/oxidation state (see Tables in main text). We note the non-octahedral environment around the iron (i.e., ligands are not directly *trans* to each other, so that movement of the iron away or towards any one particular ligand does not necessarily affect other Fe-ligand distances).

When discussing geometry optimization data of dioxygen / superoxo/ peroxo / hydroperoxo / oxo-hydroxo complexes, the following conventions will be used throughout. In end-on (monodentate) $O_2(H)$ ligands, the Fe-ligated oxygen atom will be labeled O1, with the other oxygen atom labeled O2. In side-on models, where the two Fe-O bond lengths are almost equal, the oxygen atom closer to the nitrogen atom labeled N1 in Figure 3 will be labeled O1, while the oxygen closer to N2 will be labeled O2. In oxo-hydroxo models, the oxo atom will be labeled O1, while the hydroxo oxygen will be labeled O2. Also, in Tables reporting partial atomic charges and excess spin densities, contributions from all of the protein-derived atoms are summed and listed under the notation “L3”.

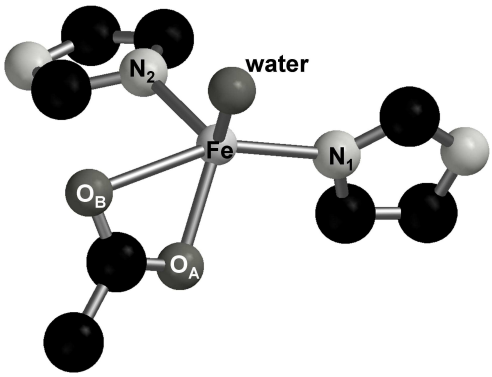

Figure 3. Geometry-optimized model **2** (S = 2, water bound), showing numbering of the protein-derived iron ligands.

Calculated energies and bond lengths for models **1** and **2** (ferrous and ferric "resting" states respectively of the NDO active site) are shown in Table 1. Table 2 lists partial atomic charges and spin densities (we note that a significant amount of spin density from the S=5/2 ferric iron appears to delocalize onto the protein derived ligands; also, the extra charge added upon reduction of **2** to **1** seems to have been delocalized to a great extent onto the protein-derived ligands). The iron site in the NDO crystal structure, 1EG9, is most likely ferrous, which is the stable oxidation state for the as-isolated enzyme in air. The crystals are also thought to have undergone reduction in the X-ray beam.[2]

Table 1.

Energies and bond distances for the ferrous and ferric "resting" states.

	Model	Energy [kcal/mol]	Fe-OH_2	O-H	Fe-N_1	Fe-N_2	Fe-O_A	Fe-O_B
1	Fe(II)-H_2O	1268564.3	2.15	0.99	2.09	2.04	1.98	2.54
2	Fe(III)-H_2O	1268327.7	2.05	0.99	2.10	2.09	2.02	2.52
1EG9	Fe-H_2O[a]	-	1.96	-	2.17	2.11	2.03	2.47

[a] Experimental geometry, from pdb entry 1EG9. The calculated Fe-O1 bond lengths suggest a ferric state in 1EG9.

Table 2.

Partial charges and spin densities (in parentheses), "resting" states.

	Model	Fe	O1	H_2O	L3[a]
1	S=2 Fe(II)-H_2O	0.76 *[3.66]*	-0.52 *[0.04]*	0.17 *[0.04]*	0.07 *[0.30]*
2	S=5/2 Fe(III)-H_2O	0.92 *[4.01]*	-0.50 *[0.08]*	0.24 *[0.09]*	0.87 *[0.90]*

[a]Sum over the protein-derived iron ligands.

"Ferrous-dioxygen" models

Calculated energies for formally ferrous-dioxygen models **3-8** are shown in Table 3. Of these models, the most stable is the side-on high-spin **8**. The recent crystal structure of dioxygen-bound naphthalene dioxygenase (with or without substrate bound)[2] suggest that the water ligand of the resting ferrous state (model **1**) is completely removed from the iron upon dioxygen binding and/or reduction to peroxide. We have nevertheless optimized geometries for models **9-17**, which are equivalents of models **3-8** but with a water ligand added. For end-on models, two coordination isomers are possible depending on whether the water ligand is placed ~trans to the N_1 nitrogen (atom numbering illustrated in Figure 3), or ~trans to N_2 (the latter models are named "exo" hereafter). Of these water models, the most stable was still the side-on high-spin (**17**). Notably, end-on models **9** and **11** converted upon geometry optimization to side-on geometries, further pointing to side-on binding of dioxygen at the NDO site as strongly favored over end-on binding. Optimized geometries for all ferrous-dioxygen models are shown in Figure S1.

A "gating" phenomenon is observed with RDOs, where dioxygen binding to the ferrous mononuclear site does not occur under physiologically-relevant conditions (but does occur under high oxygen pressure[2]) unless substrate is present *and* the nearby electron-donating Rieske site is reduced. With support from MCD and ENDOR studies, it has been argued that the gating phenomenon has a purely *structural* explanation. That is, substrate binding and reduction of the Rieske site would induce structural changes at the mononuclear site, removing one or two solvent molecules from the iron coordination sphere, thus providing open coordination positions for dioxygen. Comparison of the energies listed in Tables 1 and 2, between models **1** (ferrous-water) and **8** (ferrous-dioxygen), shows that these two states of the NDO active site have nearly equal energies (if one accounts for

the energies of free O_2 and free H_2O; zero-point vibrational energy corrections[3] and solvation would be needed for an exact comparison here). We can only hypothesize, based on these partial results, that dioxygen binding to ferrous NDO may not provide a driving force for the NDO catalytic cycle. Then, considering the high[4] $[H_2O]/[O_2]$ ratio under typical experimental and physiological conditions encountered by Rieske dioxygenases, the equilibrium between **1** and **8** would always be displaced entirely towards **1** unless external factors (such as substrate binding and reduction of the Rieske site, or increased dioxygen concentration[2]) displace it towards **8**. Then, the $[H_2O]/[O_2]$ ratio would be at least as important as previously proposed factors in "gating" O_2 access to the iron.

Table 3.

Calculated energies, "ferrous-dioxygen".

Nr.	Model	Energy [kcal/mol][a]
3	S=0 $[Fe\text{-}O_2]^{2+}$ end-on	19.8
4	S=1 $[Fe\text{-}O_2]^{2+}$ end-on	8.7
5	S=2 $[Fe\text{-}O_2]^{2+}$ end-on	9.4
6	S=0 $[Fe\text{-}O_2]^{2+}$ side-on	22.0
7	S=1 $[Fe\text{-}O_2]^{2+}$ side-on	9.9
8	S=2 $[Fe\text{-}O_2]^{2+}$ side-on	0.0
9	S=0 $[Fe\text{-}O_2]^{2+}$ end-on, + H_2O	*Side-on* (**12**)
10	S=1 $[Fe\text{-}O_2]^{2+}$ end-on, + H_2O	-47986.1
11	S=2 $[Fe\text{-}O_2]^{2+}$ end-on, + H_2O	*Side-on* (**14**)
12	S=0 $[Fe\text{-}O_2]^{2+}$ end-on, + H_2O, exo	-47980.6
13	S=1 $[Fe\text{-}O_2]^{2+}$ end-on, + H_2O, exo	-47981.3
14	S=2 $[Fe\text{-}O_2]^{2+}$ end-on, + H_2O, exo	-47981.0
15	S=0 $[Fe\text{-}O_2]^{2+}$ side-on, + H_2O	-47976.0
16	S=1 $[Fe\text{-}O_2]^{2+}$ side-on, + H_2O	-47985.6
17	S=2 $[Fe\text{-}O_2]^{2+}$ side-on, + H_2O	-47992.3

[a] Energy of model **8** (-1314962.8 kcal/mol) taken as arbitrary reference.

As shown in Table 4, in model **17**, as well as in two other less stable "extra water" models, the Fe-water distance is in fact very long, suggesting that the extra water ligand is in fact completely removed from the iron upon dioxygen binding.[3] These results not only agree with the absence of

a water ligand in the NDO "dioxygen-bound" crystal structures,[2] but also indicate these crystal structures to be placed on the most favored potential energy surface at the NDO active site (i.e., likely to be involved in the NDO catalytic cycle). Based on the above considerations, water can be excluded as a ligand to the (formally) ferrous-dioxygen form of the NDO active site.

Complexes of ferrous iron with dioxygen are often interpreted as containing a paramagnetic ferric center (S=1/2 in heme complexes) antiferromagnetically coupled to superoxide. The extremely long (1.36 Å) O-O bond of model **8** is at the upper limit of typical metal-superoxo complexes,[5] and may in fact be taken as proof of a peroxo ligand.[6] The Lowdin bond order of 1.45 is clearly indicative of a superoxo moiety, and partial atomic charges and spin densities listed in Table 5 are consistent with this interpretation. Such a long O-O bond in a ferric-superoxo system is, to our knowledge, theoretically and experimentally unprecedented. The crystal structure of ferrous NDO reacted with dioxygen[2] showed a 1.40-Å O-O bond, which, despite a relatively low resolution, the authors proposed to be indicative of a ferric-peroxo state. Our calculated 1.36-Å O-O bond now indicates the crystal structure data to also be consistent with a ferric-superoxo formulation. The Fe-O bonds of model **8** (1.83, 1.90 Å) are shorter than those observed in the substrate-free NDO-dioxygen crystal structure (2.2 and 2.3 Å), but are consistent with those observed in the crystal structure of the substrate-bound, dioxygen-bound NDO crystal structure (1.8, 2.0 Å).[2]

Table 4.

Bond distances, "ferrous-dioxygen". Lowdin bond orders are shown in parentheses, for selected models.

	Model	Fe-O1	Fe-$O2^b$	O1-O2	Fe-OH_2	Fe-N_1	Fe-N_2	Fe-O_A	Fe-O_B
3	S=0 $[Fe\text{-}O_2]^{2+}$ end-on	1.72	2.66	1.27	-	2.30	2.02	1.95	2.36
4	S=1 $[Fe\text{-}O_2]^{2+}$ end-on	1.78	2.75	1.26	-	2.14	2.09	2.00	2.48
5	S=2 $[Fe\text{-}O_2]^{2+}$ end-on	1.87	2.90	1.28	-	2.09	2.19	2.02	2.46
6	S=0 $[Fe\text{-}O_2]^{2+}$ side-on	1.76	1.96	1.33	-	2.14	2.14	2.04	2.49

Table 4. - continued

7	S=1 $[Fe\text{-}O_2]^{2+}$ side-on	1.88	1.85	1.34	-	2.19	2.12	2.00	2.44
8	S=2 $[Fe\text{-}O_2]^{2+}$ side-on[a]	1.83 (0.99)	1.90 (0.92)	1.36 (1.45)	-	2.23	2.10	2.05	2.42
9	S=0 $[Fe\text{-}O_2]^{2+}$ end-on + H_2O	-	-	-	-	-	-	-	-
10	S=1 $[Fe\text{-}O_2]^{2+}$ end-on + H_2O	1.84	2.82	1.28	2.15	2.24	2.15	2.15	2.46
11	S=2 $[Fe\text{-}O_2]^{2+}$ end-on + H_2O	-	-	-	-	-	-	-	-
12	S=0 $[Fe\text{-}O_2]^{2+}$ end-on + H_2O, exo	1.74	2.65	1.29	2.06	2.12	2.24	2.05	2.51
13	S=1 $[Fe\text{-}O_2]^{2+}$ end-on + H_2O, exo	1.87	2.85	1.25	2.58	2.12	2.14	2.06	2.52
14	S=2 $[Fe\text{-}O_2]^{2+}$ end-on + H_2O, exo	1.85	2.96	1.27	2.66	2.12	2.12	2.04	2.51
15	S=0 $[Fe\text{-}O_2]^{2+}$ end-on + H_2O	1.82	1.89	1.34	2.06	2.19	2.11	2.23	2.54
16	S=1 $[Fe\text{-}O_2]^{2+}$ side-on + H_2O	1.85	1.89	1.34	2.03	2.17	2.09	2.29	2.59
17	S=2 $[Fe\text{-}O_2]^{2+}$ end-on + H_2O	1.85	1.93	1.35	2.41	2.17	2.19	2.15	2.51

[a] Calculated Lowdin bond orders in parentheses. [b]Range of Fe-O-O angles in end-on models: 121-143.

Table 5.

"Ferrous-dioxygen": partial charges and spin densities (the latter shown in brackets).

	Model	Fe	O1	O2	OO(H)	H_2O	L3[a]
3	S=0 $[Fe\text{-}O_2]^{2+}$ end-on	0.61	-0.01	-0.12	-0.13	-	0.52
4	S=1 $[Fe\text{-}O_2]^{2+}$ end-on	0.72 *[2.67]*	-0.02 *[-0.37]*	-0.07 *[-0.61]*	-0.09 *[-0.98]*	-	0.37 *[0.35]*
5	S=2 $[Fe\text{-}O_2]^{2+}$ end-on	0.82 *[3.72]*	-0.09 *[0.03]*	-0.08 *[-0.23]*	-0.17 *[-0.20]*	-	0.23 *[0.48]*
6	S=0 $[Fe\text{-}O_2]^{2+}$ side-on	0.66	-0.06	-0.14	-0.20	-	0.54
7	S=1 $[Fe\text{-}O_2]^{2+}$ side-on	0.66 *[1.45]*	-0.10 *[0.28]*	-0.11 *[0.30]*	-0.21 *[0.58]*	-	0.55 *[-0.03]*
8	S=2 $[Fe\text{-}O_2]^{2+}$ side-on	0.78 [3.22]	-0.09 [0.24]	-0.12 [0.15]	-0.21 [0.39]	-	0.43 [0.39]
9	S=0 $[Fe\text{-}O_2]^{2+}$ end-on + H_2O	-	-	-	-	-	-
10	S=1 $[Fe\text{-}O_2]^{2+}$ end-on + H_2O	0.75 [2.88]	-0.08 [-0.42]	-0.04 [-0.71]	-0.12 [-1.13]	0.12 [0.02]	0.25 [0.25]
11	S=2 $[Fe\text{-}O_2]^{2+}$ end-on + H_2O	-	-	-	-	-	-
12	S=0 $[Fe\text{-}O_2]^{2+}$ end-on + H_2O exo	0.60	-0.02	-0.20	-0.22	0.33	0.29
13	S=1 $[Fe\text{-}O_2]^{2+}$ end-on + H_2O exo	0.74 [2.95]	-0.03 [-0.51]	-0.05 [-0.74]	-0.08 [-1.25]	0.10 [0.01]	0.24 [0.26]
14	S=2 $[Fe\text{-}O_2]^{2+}$ end-on + H_2O exo	0.79 [3.52]	-0.09 [-0.03]	-0.09 [0.11]	-0.18 [0.08]	0.09 [0.01]	0.30 [0.39]
15	S=0 $[Fe\text{-}O_2]^{2+}$ end-on + H_2O	0.59	-0.13	-0.12	-0.25	0.28	0.38
16	S=1 $[Fe\text{-}O_2]^{2+}$ side-on + H_2O	0.59 [1.34]	-0.12 [0.24]	-0.11 [0.28]	-0.23 [0.52]	0.29 [-0.01]	0.45 [0.15]
17	S=2 $[Fe\text{-}O_2]^{2+}$ end-on + H_2O	0.77 [3.23]	-0.13 [0.12]	-0.14 [0.22]	-0.27 [0.34]	0.15 [0.04]	0.35 [0.39]

[a]sum over the protein-derived iron ligands.

Finally, we note that while nitric oxide (NO) is widely used as a probe for ferrous sites of heme non-heme iron oxygen-reacting proteins (including RDOs), O_2 and NO seem to bind in completely different manners to the Rieske dioxygenase active sites: side-on vs. end-on, and with different effects on the X-O bond (X=N,O) upon binding of the diatomic XO to the iron.

"Ferric-peroxo"

Of the formally ferric-peroxo models **18-23** (Table 6), side-on S=3/2 (**22**) and S=5/2 (**23**) models are the most stable. All experimentally-characterized non-heme ferric-peroxo complexes are in fact known to be S=5/2 side-on bound (see, however[6]).

Table 6.

Calculated energies, "ferric-peroxo".

Nr.	Model	Energy [kcal/mol]
18	S=1/2 $[Fe\text{-}O_2]^+$ end-on	17.9
19	S=3/2 $[Fe\text{-}O_2]^+$ end-on	13.6
20	S=5/2 $[Fe\text{-}O_2]^+$ end-on	*side-on*[b]
21	S=1/2 $[Fe\text{-}O_2]^+$ side-on	13.6
22	S=3/2 $[Fe\text{-}O_2]^+$ side-on	0.0
23	S=5/2 $[Fe\text{-}O_2]^+$ side-on	0.6
24	S=1/2 $[Fe\text{-}O_2]^+$ side-on, + H_2O	-47970.3
25	S=3/2 $[Fe\text{-}O_2]^+$ side-on, + H_2O	-47981.5
26	S=5/2 $[Fe\text{-}O_2]^+$ side-on, + H_2O	-47990.6

[a] Energy of model **22** (-1315099.7kcal/mol) taken as arbitrary reference. [b]geometry optimization resulted in a side-on geometry.

In agreement with recent crystal structures of dioxygen-reacted ferrous NDO,[2] data in Tables 3 and 4 suggests that, upon binding to the ferrous NDO mononuclear site, dioxygen would completely displace the water ligand. Immediately after, or concerted with, its formation, the ferrous-dioxygen complex at the mononuclear site is expected to be reduced by an electron received from the nearby (~12 Å) Rieske site. Resulted from this reduction would be a formally ferric-peroxo species. To test whether this electron transfer could conceivably be coupled to re-

binding of a water ligand to iron, we have optimized geometries for models **24-26**. These models were constructed from models **21-23** by forcing a water ligand onto the peroxo-ligated iron (Fe-OH_2 starting distance as low as 1.6 Å). Of these "extra water" models, side-on S=5/2 model **26** was the most stable. However, as shown in Table 7, the Fe-water distance in **26** was very long, indicating that water is not a viable ligand to a putative ferric-peroxo complex at the NDO mononuclear site.

Energetically-favored models **23** and **26** feature O-O bond lengths and bond orders consistent with a ferric-peroxo formulation (cf. Table 7). Inclusion of an extra water molecule (models **24-26**) results in hydrogen bonding of this water molecule to the peroxo ligand, and in some degree of lengthening of the Fe-O bonds. The Fe-O and O-O bonds in model **23** are in fact a very good match for those found in the crystal structure of the dioxygen-bound, substrate-bound NDO,[2] supporting the previous assignment of this crystal structure as a ferric-peroxo species (nevertheless, as shown above, a ferric-superoxo description cannot be completely ruled out). Some predictions on the electronic absorption spectrum of a putative ferric-peroxo complex at the NDO active site are made in a separate section below.

A comparison of partial atomic charges in Tables 5 and 8 shows the added electron (upon going from formally ferric-superoxo **8** to formally ferric-peroxo **23**) to reside mainly on the dioxygen ligand and on the protein-derived ligands ("L3" in Tables).

Table 7.

Bond distances, "ferric-peroxo". Lowdin bond orders are shown in parentheses for selected models.

	Model	Fe-O1	Fe-O2	O1-O2	Fe-OH_2	O-H[a]	Fe-N_1	Fe-N_2	Fe-O_A	Fe-O_B
18	S=1/2 $[Fe\text{-}O_2]^+$ end-on	1.73	2.80	1.32	-	-	2.08	2.17	2.08	2.55
19	S=3/2 $[Fe\text{-}O_2]^+$ end-on	1.79	2.77	1.34	-	-	2.08	2.15	2.08	2.55
20	S=5/2 $[Fe\text{-}O_2]^+$ end-on	-	-	-	-	-	-	-	-	-

Table 7 - continued										
21	S=1/2 $[Fe\text{-}O_2]^+$ side-on	1.81	1.91	1.39	-	-	2.10	2.22	2.10	2.54
22	S=3/2 $[Fe\text{-}O_2]^+$ side-on	1.85	1.85	1.41	-	-	2.23	2.22	2.14	2.45
23	S=5/2 $[Fe\text{-}O_2]^+$ side-on[b]	1.92 (0.77)	1.95 (0.74)	1.43 (1.28)	-	-	2.23	2.30	2.11	2.45
24	S=1/2 $[Fe\text{-}O_2]^+$ side-on, + H_2O	1.90	1.88	1.42	2.05	1.80	2.20	2.08	2.39	2.62
25	S=3/2 $[Fe\text{-}O_2]^+$ side-on, + H_2O	1.95	1.85	1.40	2.53	1.89	2.15	2.27	2.24	2.57
26	S=5/2 $[Fe\text{-}O_2]^+$ side-on, + H_2O	2.02	1.94	1.42	2.45	2.06	2.26	2.24	2.19	2.45

[a]Distance from peroxo oxygen to water proton. [b]calculated Lowdin bond orders, in parentheses.

A

Table 8.

Partial charges and spin densities, "ferric-peroxo".

	Model	Fe	O1	O2	O_2	H_2O	L3
18	S=1/2 $[Fe\text{-}O_2]^+$ end-on	0.59 [1.41]	-0.14 [-0.18]	-0.29 [-0.29]	-0.41 [-0.47]	-	-0.17 [0.06]
19	S=3/2 $[Fe\text{-}O_2]^+$ end-on	0.68 [2.78]	-0.18 [0.08]	-0.33 [-0.05]	-0.51 [0.03]	-	-0.17 [0.19]
20	S=5/2 $[Fe\text{-}O_2]^+$ end-on	-	-	-	-	-	-
21	S=1/2 $[Fe\text{-}O_2]^+$ side-on	0.62 *[0.85]*	-0.23 *[0.09]*	-0.30 *[0.06]*	-0.53 *[0.15]*	-	-0.09 *[0.00]*
22	S=3/2 $[Fe\text{-}O_2]^+$ side-on	0.73 *[2.64]*	-0.26 *[0.12]*	-0.29 *[0.13]*	-0.55 *[0.25]*	-	-0.18 *[0.11]*

Table 8. - continued							
23	S=5/2 $[Fe\text{-}O_2]^+$ side-on	0.81 *[3.80]*	-0.30 *[0.51]*	-0.34 *[0.47]*	-0.61 *[0.98]*	-	-0.20 *[0.22]*
24	S=1/2 $[Fe\text{-}O_2]^+$ sideon, + H_2O	0.56 *[0.90]*	-0.35 *[-0.01]*	-0.27 *[0.08]*	-0.62 *[0.07]*	0.18 *[-0.01]*	-0.12 *[0.02]*
25	S=3/2 $[Fe\text{-}O_2]^+$ side-on, + H_2O	0.44 *[2.65]*	-0.28 *[0.10]*	-0.10 *[0.03]*	-0.38 *[0.13]*	0.08 *[0.04]*	-0.14 *[0.18]*
26	S=5/2 $[Fe\text{-}O_2]^+$ side-on, + H_2O	0.78 [3.79]	-0.39 [0.44]	-0.30 [0.50]	-0.69 [0.94]	0.11 [0.03]	-0.38 [0.24]

Ferric-hydroperoxo

Of the ferric-hydroperoxo models **27-29** (cf. Table 9), the most stable was found to be S=5/2 end-on **29**. Attempts to geometry-optimize side-on versions of models **27-29** invariantly resulted in end-on geometries. The possibility of water re-ligation to the active site was also considered (models **30-35**). As with the ferric-superoxo models discussed above, two geometries of coordination with the extra water exist. Of these "extra water" models, the most stable was end-on S=5/2 model **35**. Almost all non-heme ferric-hydroperoxo complexes characterized to date are low-spin.[3,7,8] However, none of these low-spin hydroperoxo complexes are able to perform dioxygenations that would mimic RDO activity (i.e., incorporation of *both* atoms of the dioxygen molecule into product). Rather, these low-spin ferric-hydroperoxo complexes undergo solvent-assisted O-O bond heterolysis and only incorporate one of the dioxygen atoms into the product of the reaction (whether it be dioxygenation or monooxygenation). The idea, that a high-spin ferric-hydroperoxo complex may be an (at least indirect) signature of an iron complex that *can* perform "true" RDO-type reactions, may deserve further investigation.

Table 9.

Energies, ferric-hydroperoxo.

Nr.	Model	Energy [kcal/mol][a]
27	S=1/2 $[Fe\text{-}O_2H]^{2+}$ end-on	19.4
28	S=3/2 $[Fe\text{-}O_2H]^{2+}$ end-on	9.4
29	S=5/2 $[Fe\text{-}O_2H]^{2+}$ end-on	0.0
30	S=1/2 $[Fe\text{-}O_2H]^{2+}$ end-on, + H_2O	-47981.8
31	S=3/2 $[Fe\text{-}O_2H]^{2+}$ end-on, + H_2O	-47980.8
32	S=5/2 $[Fe\text{-}O_2H]^{2+}$ end-on, + H_2O	-47990.3
33	S=1/2 $[Fe\text{-}O_2H]^{2+}$ end-on, + H_2O, exo	-47983.1
34	S=3/2 $[Fe\text{-}O_2H]^{2+}$ end-on, + H_2O, exo	-47980.3
35	S=5/2 $[Fe\text{-}O_2H]^{2+}$ end-on, + H_2O, exo	-47991.9

[a] Energy of model **29** (-1315353.9 kcal/mol) taken as arbitrary reference.

The calculated bond lengths (cf. Table 10) in the NDO ferric-hydroperoxo models are consistent with previous experimental and theoretical data on ferric-hydroperoxo complexes. The Fe-O and O-O bonds in model **29** are clearly shorter than those previously predicted for a S=5/2 ferric-hydroperoxo complex at the active site of superoxide reductase (SOR). The short O-O bond is instead reminiscent of the S=5/2 Fe-O-OH moiety in hemerythrin.

Table 10.

Bond distances, ferric-hydroperoxo.

	Model	Fe-O1	Fe-O2	O1-O2	Fe-OH_2	Fe-N_1	Fe-N_2	Fe-O_A	Fe-O_B
27	S=1/2 [Fe-O_2H]$^{2+}$ end-on	1.70	2.88	1.50	-	2.21	2.10	2.02	2.43
28	S=3/2 [Fe-O_2H]$^{2+}$ end-on	1.76	2.79	1.47	-	2.15	2.13	2.01	2.48
29	S=5/2 [Fe-O_2H]$^{2+}$ end-on	1.88	2.82	1.43	-	2.15	2.14	2.02	2.47
30	S=1/2 [Fe-O_2H]$^{2+}$ end-on, + H_2O	1.78	2.77	1.47	2.07	2.17	2.13	2.12	2.50
31	S=3/2 [Fe-O_2H]$^{2+}$ end-on, + H_2O	1.81	2.92	1.44	2.04	2.43	2.11	2.26	2.36
32	S=5/2 [Fe-O_2H]$^{2+}$ end-on, + H_2O	1.95	2.75	1.45	2.26	2.28	2.16	2.10	2.40
33	S=1/2 [Fe-O_2H]$^{2+}$ end-on, + H_2O, exo	1.75	2.75	1.55	2.04	2.13	2.24	2.07	2.51
34	S=3/2 [Fe-O_2H]$^{2+}$ end-on, + H_2O, exo	1.78	2.80	1.45	2.41	2.19	2.16	2.14	2.49
35	S=5/2 [Fe-O_2H]$^{2+}$ end-on, + H_2O, exo	1.91	2.80	1.44	2.84	2.19	2.15	2.10	2.47

A comparison of data in Tables 2,5,8 and 11 reveals a role for "L3" (the protein-derived ligands) as a charge buffer. Namely, changes in overall oxidation states of the models are clearly reflected in changes in the partial atomic charges of L3. Thus, starting with the ferric resting state (**2**), reduction to the ferrous form (**1**) results in a significant increase of electron

density on L3. Dioxygen binding (**8**) again draws electrons out of L3, as dioxygen needs extra electron density to achieve a superoxo state (much more electron density is withdrawn from L3 than from iron). Reduction of this formally ferric-superoxo complex to the ferric-peroxo **23** leads to an increase of charge density on L3. Finally, the added proton upon formation of the ferric-hydroperoxo induces better localization of the charge density on the peroxo atoms, resulting in a decrease of charge density on L3. Such an analysis of the role of the supposedly "innocent" iron ligands in a ferric → ferrous → ferrous-dioxygen → ferric-peroxo → ferric-hydroperoxo chain of reactions is to our knowledge unprecedented for non-heme iron complexes, and it draws an unforeseen parallel to similar heme complexes, where the porphyrin is thought to hold the key to dioxygen activation, due to its ability to store oxidizing equivalents (ability thought to be unique to highly delocalized macrocycles).[9]

Table 11.

Partial charges and spin densities, ferric-hydroperoxo.

	Model	Fe	O1	O2	OOH	H_2O	L3
27	S=1/2 [Fe-O_2H]$^{2+}$ end-on	0.70 [1.04]	-0.23 [-0.02]	-0.27 [-0.05]	-0.17 [-0.07]	-	0.47 [0.03]
28	S=3/2 [Fe-O_2H]$^{2+}$ end-on	0.79 [2.62]	-0.24 [0.17]	-0.28 [0.05]	-0.18 [0.22]	-	0.39 [0.16]
29	S=5/2 [Fe-O_2H]$^{2+}$ end-on	0.90 [3.95]	-0.29 [0.44]	-0.25 [0.11]	-0.20 [0.55]	-	0.30 [0.50]
30	S=1/2 [Fe-O_2H]$^{2+}$ end-on, + H_2O	0.64 [0.72]	-0.30 [0.25]	-0.23 [0.09]	-0.20 [0.34]	0.26 [-0.01]	0.30 [-0.05]
31	S=3/2 [Fe-O_2H]$^{2+}$ end-on, + H_2O	0.78 [2.72]	-0.32 [0.09]	-0.21 [-0.02]	-0.20 [0.07]	0.26 [0.02]	0.16 [0.19]
32	S=5/2 [Fe-O_2H]$^{2+}$ end-on, + H_2O	0.88 [3.96]	-0.34 [0.40]	-0.26 [0.10]	-0.26 [0.50]	0.16 [0.05]	0.22 [0.49]
33	S=1/2 [Fe-O_2H]$^{2+}$ end-on, + H_2O, exo	0.65 [0.85]	0.23 [0.22]	0.35 [0.02]	-0.23 [0.24]	0.23 [0.00]	0.35 [-0.09]
34	S=3/2 [Fe-O_2H]$^{2+}$ end-on, + H_2O, exo	0.78 [2.65]	-0.23 [0.14]	-0.25 [0.02]	-0.11 [0.16]	0.11 [0.01]	0.22 [0.18]
35	S=5/2 [Fe-O_2H]$^{2+}$ end-on, + H_2O, exo	0.92 [3.95]	-0.35 [0.42]	-0.22 [0.12]	-0.25 [0.54]	0.09 [0.02]	0.22 [0.49]

High-valent (oxo) intermediates

End-on hydroperoxo complexes of non-heme iron model compounds have been shown to undergo O-O bond cleavage and generate catalytically competent ferryl-oxo or perferryl-oxo complexes.[10] In these model compound hydroperoxides, O-O bond cleavage is facilitated by an iron-bound (activated) water molecule, which donates a proton to the non-iron bound oxygen atom of the hydroperoxo ligand, generating water and a (per)ferryl-oxo-hydroxo compound (oxo atom derived from hydroperoxide, hydroxo atom derived from solvent), which further performs dioxygenation of various organic substrates. The dioxygenated product in these model compounds contains one peroxide-derived oxygen atom and one solvent-derived oxygen atom. We have examined the feasibility of related perferryl-oxo-hydroxo complexes at the NDO active site by optimizing the geometries of "side-on hydroperoxo" models whose starting geometries featured O-O "bond" lengths of 2.6 Å and Fe-O bond lengths of 1.80 Å. Two isomers can exist for these oxo-hydroxo complexes: one with the oxo ligand closer to the N2 iron ligand (and closer to the substrate binding site), and one with the hydroxo ligand closer to the N2 iron ligand (the latter isomer will be referred to as "exo").

Table 12.

Energies, "perferryl-oxo-hydroxo".

Nr.	Model	Energy [kcal/mol][a]
36	S=1/2 $[Fe(O)(OH)]^{2+}$	-25.2
37	S=3/2 $[Fe(O)(OH)]^{2+}$	-1.4
38	S=5/2 $[Fe(O)(OH)]^{2+}$	9.8
39	S=1/2 $[Fe(O)(OH)]^{2+}$ exo	9.9
40	S=3/2 $[Fe(O)(OH)]^{2+}$ exo	-1.2
41	S=5/2 $[Fe(O)(OH)]^{2+}$ exo	5.7

[a] Energy of *ferric-hydroperoxo* model **29** (-1315353.9 kcal/mol) taken as arbitrary reference.

Tables 12 and 13 reveal that "perferryl-oxo-hydroxo" complexes (of which low-spin model **36** is the most stable) at the NDO active site are indeed feasible. The energies of such complexes are comparable to (and, for model **36**, even lower than) those of their isomers, the ferric-hydroperoxo complexes. Calculated geometric and electronic parameters are given in Tables 13 and 14, and they are consistent with other examples of high-vaent iron complexes.[11-14]

Table 13.

Bond distances, "perferryl-oxo-hydroxo".

	Model	Fe-O1	Fe-O2	O1-O2	O-H	Fe-N_1	Fe-N_2	Fe-O_A	Fe-O_B
36	S=1/2 $[Fe(O)(OH)]^{2+}$	1.58	1.82	2.54	0.96	2.02	2.26	2.27	2.69
37	S=3/2 $[Fe(O)(OH)]^{2+}$	1.65	1.81	2.52	0.99	2.11	2.30	2.14	2.55
38	S=5/2 $[Fe(O)(OH)]^{2+}$	1.66	1.88	2.53	0.99	2.12	2.08	2.42	2.71
39	S=1/2 $[Fe(O)(OH)]^{2+}$ exo	1.58	1.81	2.71	0.99	1.96	2.13	2.45	2.84
40	S=3/2 $[Fe(O)(OH)]^{2+}$ exo	1.65	1.81	2.50	0.99	2.12	2.30	2.13	2.54
41	S=5/2 $[Fe(O)(OH)]^{2+}$ exo	1.67	1.83	2.52	0.98	2.15	2.18	2.43	2.68

Table 14.

Partial charges and spin densities, "ferryl-oxo-hydroxo".

	Model	Fe	O1	O2	OH	L3
36	S=1/2 $[Fe(O)(OH)]^{2+}$	0.71 [0.88]	-0.27 [-0.16]	-0.38 [0.28]	-0.04 [0.27]	0.60 [0.03]
37	S=3/2 $[Fe(O)(OH)]^{2+}$	0.73 [2.22]	-0.30 [0.79]	-0.37 [0.25]	-0.04 [0.25]	0.61 [-0.26]
38	S=5/2 $[Fe(O)(OH)]^{2+}$	0.78 [2.94]	-0.34 [0.76]	-0.42 [0.44]	-0.09 [0.44]	0.66 [0.86]
39	S=1/2 $[Fe(O)(OH)]^{2+}$ exo	0.70 [0.67]	-0.21 [0.24]	-0.46 [-0.04]	-0.12 [-0.04]	0.63 [0.13]
40	S=3/2 $[Fe(O)(OH)]^{2+}$ exo	0.73 [2.19]	-0.27 [0.80]	-0.39 [0.25]	-0.06 [0.25]	0.60 [-0.24]
41	S=5/2 $[Fe(O)(OH)]^{2+}$ exo	1.08 [3.12]	-0.64 [0.60]	-0.58 [0.21]	-0.26 [0.21]	0.82 [1.07]

Electronic absorption spectra of reactive intermediates

In order to provide further support for on-going efforts of experimentally characterizing the reactive intermediates that we have described at the DFT level, we have attempted to predict electronic spectra of reactive intermediates at the NDO active site, using ZINDO/S-CI on DFT-optimized geometries.[15]

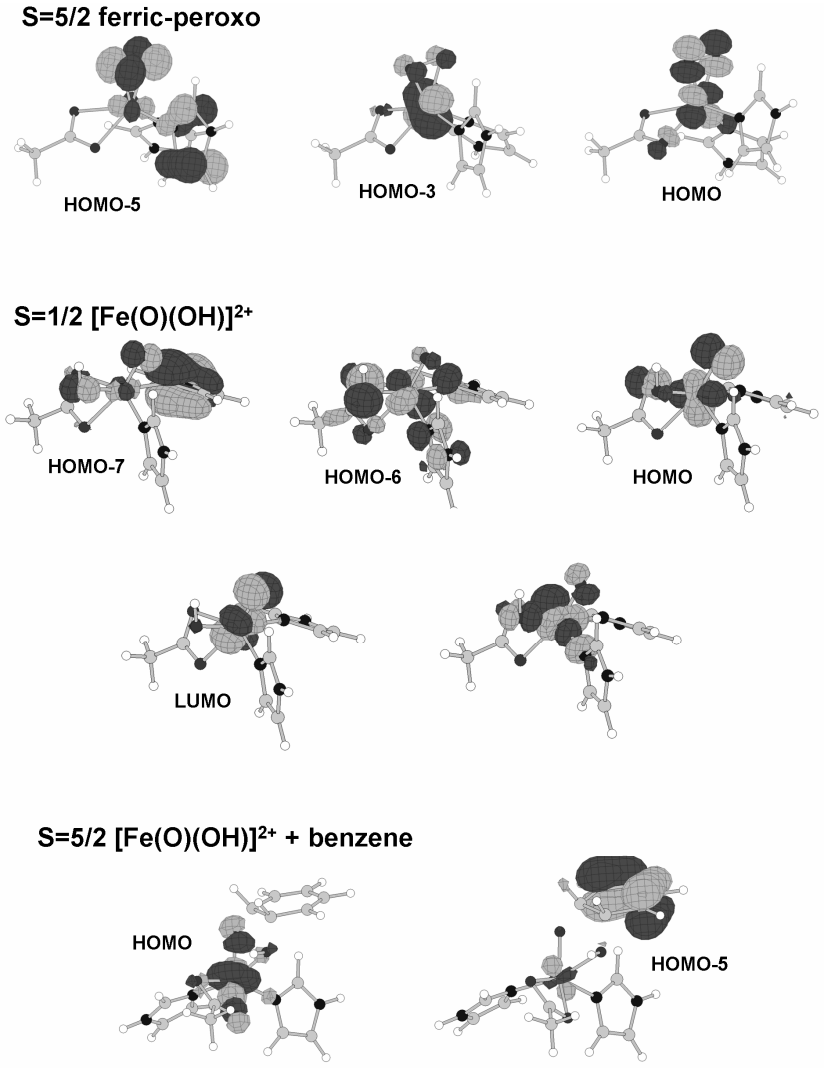

Figure 4. Main orbitals predicted to be involved in the electronic transitions in the visible region of the UV-VIS spectra for selected reactive intermediates at the NDO active site.

Ferric-peroxo complexes generally exhibit peroxo→Fe(III) charge transfer (CT) bands in the electronic absorption spectrum, at ~500-600 nm (ε~2000 $M^{-1}cm^{-1}$).[7,8] Histidine→Fe(III) CT bands are expected around 300 nm. Exceptions do exist, where relatively intense peroxo→Fe(III) CT are no longer observable at ~500-600 nm.[6] Model **23** (S=5/2 side-on ferric peroxo)

appears to be one such exception, due to the good overlap between the peroxo and histidine $\pi^{(*)}$ orbitals. As shown in Figure 4, the O-O bond in **23** is roughly perpendicular to one of the imidazole planes, and parallel to the other imidazole plane. The calculated electronic absorption spectrum featured stronger bands between 300 and 350 nm (oscillator strengths ~ 0.01 and 0.005), with histidine→Fe(III) and peroxo→Fe(III) CT character, and a weaker band at ~450 nm (oscillator strength ~0.001), with the same LMCT features (HOMO-5→HOMO-3, HOMO-5→HOMO). The main orbitals involved in these electronic transitions are shown in Figure 4. To test our hypothesis, that symmetry-based mixing or peroxo and imidazole orbitals leads to weakening of the peroxo→Fe(III) absorption in the visible region of the UV-VIS spectrum, we have also calculated the optical spectrum of a "manually" modified version of model **23**, where the peroxo moiety was reoriented to form angles of ~45° with both imidazole planes. Indeed, the oscillator strength of the band at 450 nm increased by an order of magnitude compared to the "true" (geometry optimized) model **23**.

The end-on ferric-hydroperoxo model does not show hydroperoxo→ ferric charge transfer absorption bands in the visible region. These transitions are mixed with carboxylate→ferric and imidazole→ferric absorptions at 260-300 nm. The absence of intense electronic absorptions in the visible region for ferric-hydroxperoxo complexes is not without precedent, and has been explained as due to dominance by other pi-bonding ligands.[6]

For the S=1/2 ferryl-oxo-hydroxo model **36**, a 10x5 excitation window in the configuration interaction leads to prediction of two absorption bands, one at ~390 nm (oscillator strength ~ 0.026) featuring histidine- and carboxylate-to-iron CT, and a group of bands centered between 560 and 700 nm (oscillator strengths at 0.0015-0.0053), featuring oxo-to-iron character, mixed with histidine- and carboxylate-to-iron CT (HOMO-6→LUMO, HOMO-7→LUMO, HOMO-6→HOMO, HOMO→LUMO+1). The corresponding orbitals are illustrated in Figure 4. When higher excitation windows were considered, the intensities of all the above bands decreased by at least a factor of 2.

For the S=5/2 "product-bound" model **45** (obtained from "reacting" the perferryl-oxo-hydroxo isomer with benzene) a strong band (oscillator strength ~0.463) is predicted at ~350 nm, featuring catechol-to-iron CT character, as shown in Figure 4 (HOMO-5→HOMO).

Considerations on the mechanism

Three different types of species have been proposed to be responsible for the highly selective dioxygenation accomplished at the Rieske dioxygenase active sites. A perferryl-oxo-hydroxo species has been proposed based on model compound studies. Alternatively, a side-on peroxo complex could transfer the two oxygen atoms onto an aromatic ring in a concerted fashion, as supported by recent crystal structures of the dioxygen and product-bound naphthalene dioxygenase.[2] A third mechanism, based on earlier crystal structure results and on molecular orbital symmetry considerations, involves an end-on Fe-O-O-R (R=substrate) complex, which would rearrange via a dioxetane structure, to yield the expected diol.[16]

A previous DFT study of the oxygenase reaction performed by a model compound has already shown that oxygenation of an organic substrate by a ferryl (but not perferryl) oxo-hydroxo complex (where the oxo atom originates from cleavage of a ferric-peroxo intermediate, and the hydroxo oxygen originates from solvent) has a relatively low energy barrier and is entirely feasible. Generation of the ferryl-oxo-hydroxo via protonation of the hydroperoxo by an iron-ligated water molecule was also found to have a low energy barrier. Substrate dihydroxylation by a number of model compounds has been shown to involve significant incorporation of water-derived oxygen atoms; this has been taken as proof of a ferryl-oxo-hydroxo mechanism. The same mechanism must not be valid with Rieske dioxygenases, where solvent-derived atoms are not incorporated into product to any detectable extent.

While the ferryl-oxo-hydroxo chemistry of the model compounds cannot be applied *ad literam* to Rieske dioxygenases, the possibility remains that a perferryl-oxo-hydroxo complex forms at the enzyme active site without solvent assistance.

It may be tempting to assume, based on inspection of the NDO crystal structures, that the NDO active site restricts the aromatic substrate from approaching the iron-bound activated oxygen atoms. These steric requirements would not affect in any way the peroxo-based mechanism, but would be incompatible with the ferryl-based mechanism for NDO. However, as already pointed out, spectroscopic evidence already exists for structural changes at the NDO active site upon substrate binding and upon changes in redox state at the nearby electron-transfer Rieske site. Such structural changes may conceivably involve removal of steric constraints for the perferryl-oxo mechanism.

Based on some partial electron density seen in an earlier crystal structure of indole-bound NDO, a non-concerted mechanism was proposed for indole dioxygenation, where an indole-peroxide would be formed at the NDO active site. This organic peroxide would then rearrange to an indole diol. We have attempted to model this non-concerted mechanism (using benzene as a substrate mimic, and S=5/2 peroxo as the oxygenating species), and found an activation barrier of 28 kcal/mol for formation of the "end-on" organic peroxide, and then an activation barrier of 36 kcal/mol for this peroxide isomerizing to an iron-bound benzene diol. These barriers are significantly higher than those calculated for the perferryl-oxo-hydroxo mechanism, and constitute further proof for a perferryl intermediate as *the* catalytically competent intermediate in RDOs. The lower barrier for organoperoxide formation than for subsequent diol formation suggests that, in the absence of protons, an organic peroxide may be trapped as an unproductive intermediate in the NDO active site, as seen in one of the NDO crystal structures.

Subsequent to completion of this work, Siegbahn and co-workers[17] reported a computational study on the mechanism of substrate oxidation by RDO, employing density functional theory (DFT). Dioxygen binding to the ferrous RDO site was found to yield a septet ground state. This spin multiplicity does not allow for combination of the S = 2 iron and S = 1 dioxygen frontier orbitals, consistent with an Fe-O bond longer than 2.50 Å, which is 0.8 Å longer than seen experimentally and computationally in better-characterized heme ferrous-dioxygen adducts.[18-20] This computed structure was decidedly in disagreement with the crystal structure of the NDO ferrous-dioxygen adduct, which featured a side-on dioxygen coordination geometry.[2] The lowest-energy side-on ferrous-dioxygen RDO isomers were calculated to be 5 and 10 kcal/mol higher in energy (S = 3 and S = 2, respectively). For the computed ferric-peroxo RDO models, the S = 5/2 and S = 3/2 states were close in energy, and featured side-on geometries. For the computed ferric-hydroperoxo RDO model, the S = 5/2 state was favored over S = 3/2 by 6-7 kcal/mol. DFT calculations indicated that this S = 5/2 ferric-hydroperoxo state was calculated to be capable of hydroxylating naphthalene in a multi-step mechanism where the highest activation barrier was 17-19 kcal/mol. O-O bond cleavage within S = 5/2 ferric-hydroperoxo [Fe(III)-OOH]$^{2+}$ was found to be prohibitively high, ~27 kcal/mol, suggesting that a perferryl-(oxo),hydroxo ([Fe(V)(O),OH]$^{2+}$) species would never form during the RDO catalytic cycle. O-O bond cleavage was calculated to be even more facile (activation barrier, 16

kcal/mol) in a ferrous-hydroperoxo model that would formally result upon one-electron reduction of ferric-hydroperoxo. The ferrous-hydroperoxo model was calculated to hydroxylate naphthalene in a stepwise mechanism where the highest activation barrier (involving initial attack on a carbon atom by the non-protonated oxygen atom of the Fe(III)-O-OH moiety) was 19 kcal/mol. A ferrous-hydroperoxo mechanism would be unprecedented in non-heme iron oxygenases; such chemistry is better known in heme enzymes and in non-heme model compounds.[21] Our results are mostly, but not completely consistent with those of Siegbahn and co-workers.[17].

CONCLUSIONS

Density functional calculations were reported here on the non-heme mononuclear iron active site of Rieske dioxygenases (RDO), and on complexes of this site with oxygen and activated oxygen species. Dioxygen binding to the high-spin ferrous center in RDOs is predicted to result in a S=2 side-on ferric-superoxo moiety, with a highly stranded O-O bond (1.36 Å). We propose a novel interpretation of the "gating" phenomenon in RDOs, suggesting that dioxygen binding to the ferrous site in the absence of substrate and of a reduced Rieske site may be primarily prevented by the high ($>2x10^{-6}$) $[H_2O]/[O_2]$ ratio, rather than by any specific steric/structural factors. One-electron reduction of the ferric-superoxo species is predicted to result in an S=5/2 or S=3/2 side-on ferric-peroxo species. Protonation of this peroxo is predicted to result in an S=5/2 ferric-hydroperoxo species, which is predicted to readily isomerize to a ferryl-oxo-hydroxo. These results are consistent with model compound studies, previous DFT calculations as well as with the recent crystal structures of dioxygen- and substrate-bound naphthalene dioxygenase. Electronic absorption spectra of the putative ferric-(hydro)peroxo, ferryl-oxo, and product-bound intermediates were predicted using ZINDO/S-CI calculations. Activation energies computed for substrate dihydroxylation by the species described in the present work; these results will be reported separately; they will indicate, contrary to the work from Siegbahn and co-workers, that formally Fe(V) species are the most likely active dihydroxylating agent in RDO's.

MATERIALS/METHODS

Geometries were optimized at the DFT level in the *Spartan 5.0* package at the University of Georgia Scientific Visualization and Molecular Graphics facility. The BP86 functional, which uses the gradient corrected exchange

functional proposed by Becke (1988)[22] and the correlation functional by Perdew (1986),[23] and the DN** numerical basis set (comparable in size to 6-31G**) were used as implemented in *Spartan*. For the SCF calculations, a fine grid was used and the convergence criteria were set to 10^{-6} (for the root-mean square of electron density) and 10^{-8} (energy), respectively. For geometry optimization, convergence criteria were set to 0.001 au (maximum gradient criterion) and 0.0003 (maximum displacement criterion). Charges and spin densities were derived from Mulliken population analyses after DFT geometry optimization. Lowdin bond orders were calculated at the BP/DN** geometries in the Spartan 02 for Windows package, at the BP/6-31G** level. ZINDO/S-CI calculations were performed on the DFT-optimized structures in the *Hyperchem 4.5* package.[2]

Active site models were built using heavy-atom coordinates from pdb entry 1EG9 (NDO + indole crystal structure, 1.60 Å resolution). All models were constructed within the Builder module of the *Spartan* package. All models contained Fe ligated by three protein-derived ligands: a carboxylate (modeled as CH_3COO^-) and two protonated (neutral) imidazoles (cf. Figure 3). The "fourth" (or fifth, if one counts the carboxylate as bidentate) ligand was water, peroxo, hydroperoxo, etc. (cf. Figures 2 and 3, and as listed in Tables, below). For selected models, an extra water ligand was introduced in addition to the dioxygen/superoxo/peroxo ligand.

ACKNOWLEDGEMENTS

Drs. I. Silaghi-Dumitrescu (UBB), Zanna Beharry, Eric Coulter and Donald M. Kurtz, Jr. (University of Georgia) are thanked for helpful discussions. This paper is dedicated to the memory of Dr. Eric D.Coulter.

REFERENCES

[1] M. Costas, M.P. Mehn, M.P. Jensen, L.J. Que, Chem. Rev., 2004, 2, 939-86.

[2] A. Karlsson, J. Parales, R. Parales, D. Gibson, H. Eklund, Science, 2003, 299, 1039-1042.

[3] A. Wada, S. Ogo, S. Nagatomo, T. Kitagawa, Y. Watanabe, K. Jitsukawa, H. Masuda, Inorg. Chem., 2002, 41, 616-618.

[4] A total of two water molecules are seen within ~3.5 Å from the iron in the NDO active site, in the crystal structure (1EG9); this is equivalent to an *effective concentration of water of >10 M* at the mononuclear site, even though this site is generally described as hydrophobic, .

[5] D.M. Kurtz, Jr., Essays in Biochemistry, 1999, 55-80.

[6] R. Silaghi-Dumitrescu, I. Silaghi-Dumitrescu, E.D. Coulter, D.M. Kurtz, Jr., Inorg. Chem., 2003, 42, 446-456.

[7] J. Girerd, F. Banse, A. Simaan, Structure and Bonding, 2000, 97, 145-176.

[8] E.I. Solomon, T.C. Brunold, M.I. Davis, J.N. Kemsley, S.K. Lee, N. Lehnert, N. Neese, A.J. Skulan, Y.S. Yang, Z. Zhou, Chem. Rev., 2000, 100, 235-350.

[9] M. Sono, M.P. Roach, E.D. Coulter, J.H. Dawson, Chem. Rev., 1996, 96, 2841-2888.

[10] A. Bassan, M. Blomberg, P. Siegbahn, L.J. Que, J. Am. Chem. Soc., 2002, 124, 11056-11063.

[11] R. Silaghi-Dumitrescu, Proc. Rom. Acad. Series B, 2006, 2-3, 95-101.

[12] R. Silaghi-Dumitrescu, Studia Univ. Babes-Bolyai, Chemia, 2005, 50, 17-21.

[13] R. Silaghi-Dumitrescu, C.E. Cooper, Dalton Trans., 2005, 3477-3482.

[14] R. Silaghi-Dumitrescu, J. Biol. Inorg. Chem., 2004, 9, 471-476.

[15] HyperChem(TM) Molecular Modelling System, Release 4.5 SGI, Hypercube; Hyperchem(TM) Molecular Modelling System, Release 5.01 for Windows, Hypercube, Inc., .

[16] V. Bui, M. Nguyen, J. Hansen, J. Baker, T. Hudlicky, Can. J. Chem., 2002, 80, 708-713.

[17] A. Bassan, M.R. Blomberg, P.E. Siegbahn, J Biol Inorg Chem, 2004, 9, 439-52.

[18] P. Rydberg, E. Sigfridsson, U. Ryde, J. Biol. Inorg. Chem., 2004, 9, 203-223.

[19] R. Silaghi-Dumitrescu, I. Silaghi-Dumitrescu, Rev. Roum. Chim., 2004, 3-4, 257-268.

[20] T.G. Spiro, M.K. Zgierski, P.M. Kozlowski, Coord. Chem. Rev., 2001, 219-221, 923-936.

[21] R. Silaghi-Dumitrescu, Arch. Biochem. Biophys., 2004, 424, 137-140.

[22] A.D. Becke, Phys. Rev., 1988, 3098-3100.

[23] J.P. Perdew, Phys. Rev., 1986, B33, 8822-8824.